A direct determination of the number of light neutrino families from e+ e- ---> neutrino anti-neutrino gamma at LEP

Adeva, B.; Adriani, O.; Aguilar-Benitez, M.; Ahlen, S.P.; Akbari, H.; Alcaraz, J.; Aloisio, A.; Alverson, G.; Linde, F.L.

Published in:
Physics Letters B

DOI:
10.1016/0370-2693(92)90877-7

Physics Letters B 275 (1992) 209–221
North-Holland

PHYSICS LETTERS B

A direct determination of the number of light neutrino families from $e^+e^- \to \nu\bar{\nu}\gamma$ at LEP

L3 Collaboration

B. Adeva [a], O. Adriani [b], M. Aguilar-Benitez [c], H. Akbari [d], J. Alcaraz [c], A. Aloisio [e], G. Alverson [f], M.G. Alviggi [e], G. Ambrosi [g], Q. An [h], H. Anderhub [i], A.L. Anderson [j], V.P. Andreev [k], T. Angelov [j], L. Antonov [ℓ], D. Antreasyan [m], P. Arce [c], A. Arefiev [n], A. Atamanchuk [k], T. Azemoon [o], T. Aziz [p], P.V.K.S. Baba [h], P. Bagnaia [q], J.A. Bakken [r], L. Baksay [s], R.C. Ball [o], S. Banerjee [p], J. Bao [d], R. Barillère [a], L. Barone [q], R. Battiston [g], A. Bay [t], F. Becattini [b], U. Becker [j,i], F. Behner [i], J. Behrens [i], S. Beingessner [u], Gy.L. Bencze [v], J. Berdugo [c], P. Berges [j], B. Bertucci [g], B.L. Betev [ℓ,i], M. Biasini [g], A. Biland [i], G.M. Bilei [g], R. Bizzarri [q], J.J. Blaising [u], P. Blömeke [w], B. Blumenfeld [d], G.J. Bobbink [x], M. Bocciolini [b], R. Bock [w], A. Böhm [w], B. Borgia [q], D. Bourilkov [ℓ], M. Bourquin [t], D. Boutigny [u], B. Bouwens [x], E. Brambilla [e], J.G. Branson [y], I.C. Brock [z], M. Brooks [aa], F. Bruyant [a], C. Buisson [ab], A. Bujak [ac], J.D. Burger [j], W.J. Burger [t], J.P. Burq [ab], J. Busenitz [s], X.D. Cai [h], M. Capell [ad], M. Caria [g], F. Carminati [b], A.M. Cartacci [b], M. Cerrada [c], F. Cesaroni [q], Y.H. Chang [j], U.K. Chaturvedi [h], M. Chemarin [ab], A. Chen [ae], C. Chen [af], G.M. Chen [af], H.F. Chen [ag], H.S. Chen [af], J. Chen [j], M. Chen [j], M.L. Chen [o], W.Y. Chen [h], G. Chiefari [e], C.Y. Chien [d], M. Chmeissani [o], C. Civinini [b], I. Clare [j], R. Clare [j], T.E. Coan [aa], H.O. Cohn [ah], G. Coignet [u], N. Colino [a], A. Contin [m,a], F. Crijns [ai], X.Y. Cui [h], T.S. Dai [j], R. D'Alessandro [b], R. de Asmundis [e], A. Degré [u], K. Deiters [j], E. Dénes [v], P. Denes [r], F. DeNotaristefani [q], M. Dhina [i], D. DiBitonto [s], M. Diemoz [q], H.R. Dimitrov [ℓ], C. Dionisi [q,a], M.T. Dova [h], E. Drago [e], T. Driever [ai], D. Duchesneau [t], P. Duinker [x], I. Duran [c], H. El Mamouni [ab], A. Engler [z], F.J. Eppling [j], F.C. Erné [x], P. Extermann [t], R. Fabbretti [aj], M. Fabre [i], S. Falciano [q], Q. Fan [h], S.J. Fan [ak], O. Fackler [ad], J. Fay [ab], M. Felcini [a], T. Ferguson [z], D. Fernandez [c], G. Fernandez [c], F. Ferroni [q], H. Fesefeldt [w], E. Fiandrini [g], J. Field [t], F. Filthaut [ai], G. Finocchiaro [q], P.H. Fisher [d], G. Forconi [t], T. Foreman [x], K. Freudenreich [i], W. Friebel [aℓ], M. Fukushima [j], M. Gailloud [am], Yu. Galaktionov [n,j], E. Gallo [b], S.N. Ganguli [p], P. Garcia-Abia [c], S.S. Gau [ae], D. Gele [ab], S. Gentile [q,a], S. Goldfarb [o], Z.F. Gong [ag], E. Gonzalez [c], A. Gordeev [n], P. Göttlicher [w], D. Goujon [t], G. Gratta [an], C. Grinnell [j], M. Gruenewald [an], M. Guanziroli [h], J.K. Guo [ak], A. Gurtu [p,a], H.R. Gustafson [o], L.J. Gutay [ac], K. Hangarter [w], A. Hasan [h], D. Hauschildt [x], C.F. He [ak], T. Hebbeker [w], M. Hebert [y], G. Herten [j], U. Herten [w], A. Hervé [a], K. Hilgers [w], H. Hofer [i], H. Hoorani [t], G. Hu [h], G.Q. Hu [ak], B. Ille [ab], M.M. Ilyas [h], V. Innocente [e,a], H. Janssen [a], S. Jezequel [u], B.N. Jin [af], L.W. Jones [o], A. Kasser [am], R.A. Khan [h], Yu. Kamyshkov [ah,n], P. Kapinos [k], J.S. Kapustinsky [aa], Y. Karyotakis [u,a], M. Kaur [h], S. Khokhar [h], M.N. Kienzle-Focacci [t], W.W. Kinnison [aa], D. Kirkby [an], S. Kirsch [aℓ], W. Kittel [ai], A. Klimentov [j,n], A.C. König [ai], O. Kornadt [w], V. Koutsenko [j,n], A. Koulbardis [k], R.W. Kraemer [z], T. Kramer [j], V.R. Krastev [ℓ], W. Krenz [w], A. Krivshich [k], J. Krizmanic [d], K.S. Kumar [ao], V. Kumar [h], A. Kunin [ao,n], G. Landi [b], K. Lanius [a], D. Lanske [w], S. Lanzano [e], P. Lebrun [ab], P. Lecomte [i], P. Lecoq [a], P. Le Coultre [i], D.M. Lee [aa], I. Leedom [f], J.M. Le Goff [a], L. Leistam [a], R. Leiste [aℓ], M. Lenti [b], E. Leonardi [q], J. Lettry [i], X. Leytens [x], C. Li [ag,h], H.T. Li [af], J.F. Li [h], P.J. Li [ak], Q. Li [h], X.G. Li [af], J.Y. Liao [ak], W.T. Lin [ae], Z.Y. Lin [ag], F.L. Linde [a,x], B. Lindemann [w], D. Linnhofer [i], R. Liu [h], Y. Liu [h], W. Lohmann [aℓ,a], E. Longo [q], Y.S. Lu [af], J.M. Lubbers [a], K. Lübelsmeyer [w], C. Luci [a], D. Luckey [m,j], L. Ludovici [q], L. Luminari [q], W.G. Ma [ag], M. MacDermott [i], P.K. Malhotra [p], R. Malik [h], A. Malinin [u,n], C. Maña [c], D.N. Mao [o], Y.F. Mao [af], M. Maolinbay [i], P. Marchesini [i], J.P. Martin [ab], L. Martinez-Laso [a], F. Marzano [q], G.G.G. Massaro [x], T. Matsuda [j], K. Mazumdar [p], P. McBride [ao], T. McMahon [ac], D. McNally [i], Th. Meinholz [w], M. Merk [ai], L. Merola [e], M. Meschini [b], W.J. Metzger [ai], Y. Mi [h], G.B. Mills [aa], Y. Mir [h], G. Mirabelli [q], J. Mnich [w], M. Möller [w], B. Monteleoni [b], R. Morand [u], S. Morganti [q], N.E. Moulai [h], R. Mount [an], S. Müller [w], A. Nadtochy [k], E. Nagy [v], M. Napolitano [e], H. Newman [an], C. Neyer [i], M.A. Niaz [h], L. Niessen [w], H. Nowak [aℓ], G. Organtini [q], D. Pandoulas [w], M. Pauluzzi [g], F. Pauss [i], G. Passaleva [b], S. Paoletti [b], S. Patricelli [e], Y.J. Pei [w], D. Perret-Gallix [u], J. Perrier [t], A. Pevsner [d], M. Pieri [b], P.A. Piroué [r], F. Plasil [ah], V. Plyaskin [n], M. Pohl [i], V. Pojidaev [n,b], N. Produit [t], J.M. Qian [o], K.N. Qureshi [h], R. Raghavan [p], G. Rahal-Callot [i], G. Raven [x], P. Razis [s], K. Read [ah], D. Ren [i], Z. Ren [h], M. Rescigno [q], S. Reucroft [f], A. Ricker [w], S. Riemann [aℓ], O. Rind [o], H.A. Rizvi [h], B.P. Roe [o], M. Röhner [w], S. Röhner [w], L. Romero [c], J. Rose [w], S. Rosier-Lees [u], R. Rosmalen [ai], Ph. Rosselet [am], A. Rubbia [j], J.A. Rubio [a,c], H. Rykaczewski [i], M. Sachwitz [aℓ,a], J. Salicio [a,c], J.M. Salicio [c], G.S. Sanders [aa], A. Santocchia [g], M.S. Sarakinos [j], G. Sartorelli [m,h], G. Sauvage [u], A. Savin [n], V. Schegelsky [k], K. Schmiemann [w], D. Schmitz [w], P. Schmitz [w], M. Schneegans [u], H. Schopper [ap], D.J. Schotanus [ai], S. Shotkin [j], H.J. Schreiber [aℓ], J. Shukla [z], R. Schulte [w], S. Schulte [w], K. Schultze [w], J. Schütte [ao], J. Schwenke [w], G. Schwering [w], C. Sciacca [e], I. Scott [ao], R. Sehgal [h], P.G. Seiler [aj], J.C. Sens [x], L. Servoli [g], I. Sheer [y], D.Z. Shen [ak], S. Shevchenko [an,n], X.R. Shi [an], K. Shmakov [n], E. Shumilov [n], V. Shoutko [n], E. Soderstrom [r], A. Sopczak [y], C. Spartiotis [d], T. Spickermann [w], P. Spillantini [b], R. Starosta [w], M. Steuer [m,j], D.P. Stickland [r], F. Sticozzi [j], H. Stone [t], K. Strauch [ao], B.C. Stringfellow [ac], K. Sudhakar [p,w], G. Sultanov [h], R.L. Sumner [r], L.Z. Sun [ag,h], H. Suter [i], R.B. Sutton [z], J.D. Swain [h], A.A. Syed [h], X.W. Tang [af], E. Tarkovsky [n], L. Taylor [f], C. Timmermans [ai], Samuel C.C. Ting [j], S.M. Ting [j], M. Tonutti [w], S.C. Tonwar [p], J. Tóth [v,a], A. Tsaregorodtsev [k], G. Tsipolitis [z], C. Tully [an], K.L. Tung [af], J. Ulbricht [i], L. Urbán [v], U. Uwer [w], E. Valente [q], R.T. Van de Walle [ai], I. Vetlitsky [n], G. Viertel [i], P. Vikas [h], U. Vikas [h], M. Vivargent [u], H. Vogel [z], H. Vogt [aℓ], G. Von Dardel [a], I. Vorobiev [n], A.A. Vorobyov [k], L. Vuilleumier [am], M. Wadhwa [h], W. Wallraff [w], C.R. Wang [ag], G.H. Wang [z], J.H. Wang [af], Q.F. Wang [ao], X.L. Wang [ag], Y.F. Wang [b], Z. Wang [h], Z.M. Wang [h,ag], A. Weber [w], J. Weber [i], R. Weill [am], T.J. Wenaus [ad], J. Wenninger [t], M. White [j], C. Willmott [c], F. Wittgenstein [a], D. Wright [r], R.J. Wu [af], S.L. Wu [h], S.X. Wu [h], Y.G. Wu [af], B. Wysłouch [j], Y.Y. Xie [ak], Y.D. Xu [af], Z.Z. Xu [ag], Z.L. Xue [ak], D.S. Yan [ak], X.J. Yan [j], B.Z. Yang [ag], C.G. Yang [af], G. Yang [h], K.S. Yang [af], Q.Y. Yang [af], Z.Q. Yang [ak], C.H. Ye [h], J.B. Ye [ag], Q. Ye [h], S.C. Yeh [ae], Z.W. Yin [ak], J.M. You [h], M. Yzerman [x], C. Zaccardelli [an], P. Zemp [i], M. Zeng [h], Y. Zeng [w], D.H. Zhang [x], Z.P. Zhang [ag,h], J.F. Zhou [w], R.Y. Zhu [an], H.L. Zhuang [af] and A. Zichichi [m,a,h]

[a] *European Laboratory for Particle Physics, CERN, CH-1211 Geneva 23, Switzerland*
[b] *INFN – Sezione di Firenze and University of Florence, I-50125 Florence, Italy*
[c] *Centro de Investigaciones Energeticas, Medioambientales y Tecnologicas, CIEMAT, E-28040 Madrid, Spain*
[d] *Johns Hopkins University, Baltimore, MD 21218, USA*
[e] *INFN – Sezione di Napoli and University of Naples, I-80125 Naples, Italy*
[f] *Northeastern University, Boston, MA 02115, USA*
[g] *INFN – Sezione di Perugia and Universitá Degli Studi di Perugia, I-06100 Perugia, Italy*
[h] *World Laboratory, FBLJA Project, CH-1211 Geneva, Switzerland*
[i] *Eidgenössische Technische Hochschule, ETH Zürich, CH-8093 Zurich, Switzerland*
[j] *Massachusetts Institute of Technology, Cambridge, MA 02139, USA*
[k] *Nuclear Physics Institute, SU-188 350 St. Petersburg, USSR*

[ℓ] Central Laboratory of Automation and Instrumentation, CLANP, Sofia, Bulgaria
[m] INFN - Sezione di Bologna, I-40126 Bologna, Italy
[n] Institute of Theoretical and Experimental Physics, ITEP, SU-117 259 Moscow, USSR
[o] University of Michigan, Ann Arbor, MI 48109, USA
[p] Tata Institute of Fundamental Research, Bombay 400 005, India
[q] INFN - Sezione di Roma and University of Rome "La Sapienza", I-00185 Rome, Italy
[r] Princeton University, Princeton, NJ 08544, USA
[s] University of Alabama, Tuscaloosa, AL 35486, USA
[t] University of Geneva, CH-1211 Geneva 4, Switzerland
[u] Laboratoire de Physique des Particules, LAPP, F-74519 Annecy-le-Vieux, France
[v] Central Research Institute for Physics of the Hungarian Academy of Sciences, H-1525 Budapest 114, Hungary
[w] I. Physikalisches Institut, RWTH, W-5100 Aachen, FRG [1]
and III. Physikalisches Institut, RWTH, W-5100 Aachen, FRG [1]
[x] National Institute for High Energy Physics, NIKHEF, NL-1009 DB Amsterdam, The Netherlands
[y] University of California, San Diego, CA 92182, USA
[z] Carnegie Mellon University, Pittsburgh, PA 15213, USA
[aa] Los Alamos National Laboratory, Los Alamos, NM 87544, USA
[ab] Institut de Physique Nucléaire de Lyon, IN2P3-CNRS/Université Claude Bernard, F-69622 Villeurbanne Cedex, France
[ac] Purdue University, West Lafayette, IN 47907, USA
[ad] Lawrence Livermore National Laboratory, Livermore, CA 94550, USA
[ae] High Energy Physics Group, Taiwan, ROC
[af] Institute of High Energy Physics, IHEP, Beijing, China
[ag] University of Science and Technology of China, Hefei, Anhui 230 029, China
[ah] Oak Ridge National Laboratory, Oak Ridge, TN 37830, USA
[ai] University of Nijmegen and NIKHEF, NL-6525 ED Nijmegen, The Netherlands
[aj] Paul Scherrer Institut (PSI), Würenlingen, Switzerland
[ak] Shanghai Institute of Ceramics, SIC, Shanghai, China
[aℓ] Institut für Hochenergiephysik, O-1615 Zeuthen-Berlin, FRG [1]
[am] University of Lausanne, CH-1015 Lausanne, Switzerland
[an] California Institute of Technology, Pasadena, CA 91125, USA
[ao] Harvard University, Cambridge, MA 02139, USA
[ap] University of Hamburg, W-2000 Hamburg, FRG

Received 18 November 1991

The L3 detector at LEP has been used to determine the number of light neutrino families by measuring the cross section of single photon even in e^+e^- collisions at energies near the Z^0 resonance. We have observed 61 single photon candidates with more than 1.5 GeV of deposited energy in the barrel electromagnetic calorimeter, for a total integrated luminosity of 3.0 pb^{-1}. From a likelihood fit to the single photon cross sections, we determine $N_\nu = 3.24 \pm 0.46$ (statistical) ± 0.22 (systematic).

1. Introduction

One of the most fundamental results obtained by the LEP experiments is the determination of the number of light neutrino families N_ν. Assuming that the only stable, weakly interacting particles are light neutrinos with standard model couplings, this number is inferred, in a nearly model-independent way, from the measurements of the invisible width extracted from the Z^0 line shape [1]. This indirect determination, for which L3 obtains $N_\nu = 3.05 \pm 0.10$, assumes that all visible decays of the Z^0 are from the charged leptonic and hadronic final states. The dominant contribution to the error comes from the uncertainty in the luminosity, but the systematics in the analysis of the hadronic and charged leptonic decay modes, taken together, also contribute significantly to the error.

In this paper we follow a complementary approach, proposed some time ago by several authors

[1] Supported by the German Bundesministerium für Forschung und Technologie.

[2], in which the number of neutrino families is counted directly by the measurement of the cross section for the process $e^+e^- \to \nu\bar{\nu}\gamma$. The signature of such events is a single photon arising from initial state radiation. The cross section can be written as [3]

$$\frac{d^2\sigma}{dE_\gamma \, d\cos\theta_\gamma} = H(E_\gamma, \cos\theta_\gamma, s)\sigma_0(s') , \quad (1)$$

where H is a radiator function for photons of energy E_γ and polar angle θ_γ, s is the square of the center of mass energy, and $\sigma_0(s')$ is the "reduced" cross section for the process $e^+e^- \to \nu\bar{\nu}$, in the new center of mass system, given by $s' = s(1 - 2E_\gamma/\sqrt{s})$. In lowest order and by approximating the W contribution by a four-point interaction, σ_0 is given by [2,3]

$$\sigma_0(s) = \frac{G_F^2 s}{12\pi}\left(2 + \frac{N_\nu(g_v^2 + g_a^2)}{(1 - s/M_Z^2)^2 + \Gamma_Z^2/M_Z^2} + \frac{2(g_v + g_a)(1 - s/M_Z^2)}{(1 - s/M_Z^2)^2 + \Gamma_Z^2/M_Z^2}\right). \quad (2)$$

The dominant term is proportional to the number of light neutrino families N_ν and represents the square of the amplitude for Z^0 production. The first term arises from the square of the W exchange diagram, which contributes only to ν_e production, and the last one is due to W–Z interference. The sum of the first and third terms contributes to the overall cross section by less than 3% in the energy range analysed in this paper [3]. The contribution to σ_0 from the term proportional to N_ν remains dominant in the case that the exact calculation is carried out including higher-order corrections.

In the past few years, experiments at PEP [4], PETRA [5] and TRISTAN [6] have measured the single photon cross section well below the Z^0 resonance. They yield a combined limit of less than 4.8 light neutrino families at 95% confidence level [6]. The measurement is optimally carried out at energies at least 4 GeV above the Z^0 mass where the ratio between the signal and QED background processes is maximum and the full width of the Z^0 resonance is exploited [2,7]. However, the LEP scanning strategy at the Z^0 resonance [1] has given less favourable conditions for our first measurements, requiring a trigger efficient for low energy photons ($E > 1$ GeV), a better knowledge of the electromagnetic energy scale and tighter control of backgrounds.

In this paper we present a measurement in L3, from data taken at LEP in 1990 at center of mass energies between 88.3 and 94.3 GeV. The corresponding integrated luminosity is 3.0 pb^{-1}.

2. The L3 detector

The L3 detector and its performance in the detection of muons, electrons and photons is described in detail elsewhere [8]. Here we only outline the features relevant to the present analysis. The detector consists of a central tracking and vertex chamber (TEC), a BGO barrel electromagnetic calorimeter, a hadron calorimeter made of uranium absorber and brass proportional wire chambers and a high precision muon chamber system. The BGO polar angle acceptance goes from 42.3° to 137.7° and is fully covered by the TEC, the muon chambers covers polar angles from 36° to 144°, and the hadron calorimeter from 6° to 174°. Between the BGO and the hadron calorimeter is a cylindrical array of 30 scintillation counters. Just in front of the hadron calorimeter endcaps, between 7° and 37°, is a lead-scintillator veto counter having a total depth of 6.5 radiation lengths. These subdetectors are installed in a 12 m inner diameter solenoidal magnet which provides a uniform magnetic field of 0.5 T parallel to the beam direction.

Around the Z^0 pole, the photons from $\nu\bar{\nu}\gamma$ have low energies with a rapidly falling spectrum. Therefore, the BGO barrel energy resolution, better than 2% for $E_\gamma > 1.5$ GeV, the BGO linearity, and the negligible uncertainty in the absolute energy scale are well-suited for the detection of such photons.

The minimum angle at which particles can be detected, critical to the suppression of QED background, is defined by the luminosity monitors. They consist of two electromagnetic calorimeters and two sets of proportional wire chambers, situated symmetrically on either side of the interaction point. Each calorimeter is a finely segemented and azimuthally symmetric array of 304 BGO crystals covering the polar angular range $24.93 < \theta < 69.94$ mrad. The energy resolution of the calorimeters is about 2% at 45 GeV, and the position resolution is 0.4 mrad in θ and 0.5° in ϕ.

Apart from the region below the minimum detection angle, there is a region (hole) about 2° wide in

θ between the luminosity monitors and the hadron calorimeters endcaps which is not covered by any detector. There is thus additional background from radiative Bhabha events when one of the particles escapes undetected through this hole.

The response of the L3 detector is modelled using the GEANT3 [9] detector simulation program which includes the effects of energy loss, multiple scattering and showering in the detector materials and in the beam pipe. Hadronic showers in the calorimeters are simulated with the GHEISHA [10] program. For each of the physical processes studied, Monte Carlo events are passed through the detector simulation program and are reconstructed by the same program that is used to reconstruct the real ones.

3. Trigger

Each BGO barrel crystal has a separate output for trigger purposes. These outputs are summed in trigger segments of 30 crystals with a segmentation of 32 in ϕ and 8 in θ. The 256 sums are sent to the trigger FERA (Fast Encoding Readout ADC) system [11] and subsequently to the first level energy trigger processor [12].

A decision to set the single photon trigger bit is made as follows. Firstly, "θ sums" (Σ_θ) and "ϕ sums" (Σ_ϕ) are calculated by summing over the trigger segment energies at constant θ and at constant ϕ, respectively. In order to suppress the contribution from coherent noise, the calculation includes only trigger segments above a 1 GeV threshold (called bias in the following). A total of 8 θ sums and 32 ϕ sums is thus obtained. Secondly, all the trigger segments above the bias are summed to obtain a total energy Σ_{TOT}. Finally, the first level trigger processor fires the single photon trigger if the following conditions are met:

$$\Sigma_\theta^{\max} > 1.5\ \mathrm{GeV}, \quad \Sigma_\phi^{\max} > 1.5\ \mathrm{GeV},$$

$$\Sigma_\theta^{\max} > 0.8\ \Sigma_{\mathrm{TOT}}, \quad \Sigma_\phi^{\max} > 0.8\ \Sigma_{\mathrm{TOT}},$$

where $\Sigma_\theta^{\max}$ and $\Sigma_\phi^{\max}$ are the largest θ sum and the largest ϕ sum, respectively. The typical trigger rate under these conditions was 0.3 Hz, mainly due to electronic noise.

A subsequent reduction by a factor of four is achieved by the level-three trigger, which makes use of the complete set of digitized data. It requires a single BGO cluster which has an energy greater than 500 MeV distributed among more than 2 and less than 80 crystals. The level-three trigger efficiency exceeds 99.9% for $\nu\bar{\nu}\gamma$ events above 1.5 GeV.

The efficiency of the single photon trigger has been studied by considering events which consists of a single electromagnetic deposit in the BGO barrel and a large energy deposit in the forward part of the detector (hadron calorimeter endcaps or luminosity detector). These events are typically radiative Bhabha events in which one of the particles remains in the beam pipe. Due to the presence of the forward energy deposit, the event will be accepted by either the single-tag luminosity trigger, which requires at least 30 GeV in one of the luminosity monitors, or the low angle energy trigger, which fires if more than 20 GeV is deposited in the veto counter and hadron calorimeter endcaps. The single-tag luminosity trigger and the low angle energy trigger are thus independent of the single photon trigger. The efficiency is then measured by checking whether or not the single photon trigger also fired. The dark black dots in fig. 1 plot the efficiency found as a function of the photon energy. The statistics of this sample is limited because the luminosity single-tag triggers were prescaled by a factor of 20 during 1990 data taking.

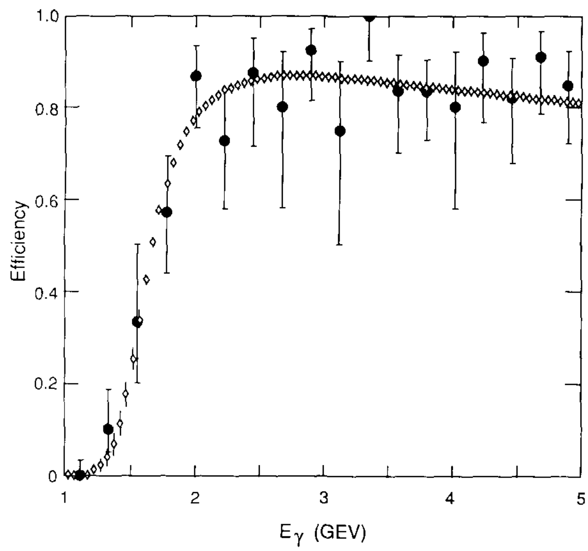

Fig. 1. Measured (circle) and simulated (diamond) trigger efficiency curve as a function of photon energy.

We therefore made a calculation through a simulation of the algorithm used by the level one trigger, taking into account inactive and noisy trigger segments and the lateral shape of the electromagnetic shower.

The main sources of trigger efficiency are:

(1) Trigger FERA energy resolution which decreases from 10% at 1 GeV to 6% at 5 GeV.

(2) Noise from the electronics in coincidence with a genuine single photon event which vetoes the trigger by the energy fraction requirement. In approximately 0.2% of events obtained by triggering on the beam crossing (such events are referred to as beam gate events below), at least one trigger segment had an energy above the 1 GeV bias.

(3) Channels not active in the trigger algorithm: during 1990 data-taking period, 10% of the BGO trigger segments were inactive.

(4) Photon showering into adjacent trigger segments where one or more channels have an energy below the 1 GeV bias, so that the effective energy of the photon may be reduced to a value below the trigger threshold; or the energy deposition pattern resulting in two or more channels above the trigger segment bias, none of which satisfies the energy fraction requirement ("self-veto").

We generated single photon events in the BGO at a given energy and angle. The simulation distributed energy among the crystals according to a parametrization determined from test beam data and took into account FERA resolution and the presence of inactive channels. Real beam gate events were superimposed on the generated events in order to reproduce the effects of FERA pedestal fluctuations and electronic noise. The application of the trigger algorithm to this sample has allowed the determination of the trigger efficiency, as a function of the photon energy and angles θ and ϕ. Fig. 1 shows this computed efficiency curve, averaged over the angular variables, as a function of the photon energy. It rises sharply at the energy threshold and reaches an almost constant value, mainly determined by the presence of inactive channels. The slight decrease above 3 GeV is due to the increased probability of the "self-veto" effect described in point (4) above. The errors correspond to extreme assumptions in the model used to compute the efficiency. They include the statistical errors on the FERA resolution and the systematic error in knowledge of the shower development in the BGO.

As can be seen from fig. 1, the two determinations of the trigger efficiency agree well within uncertainties. In what follows, we use the stimulated trigger efficiency. From a comparison between the simulated curve and the experimental points of this figure, we estimate an absolute systematic error for the trigger efficiency of ± 0.04.

4. Single photon sample

For $Z^0 \to \nu\bar{\nu}\gamma$ events, our selection aims at isolating events where only a single electromagnetic energy deposit in the BGO is seen, with no other particle in the rest of the detector. Candidates are selected by requiring the following:

(1) There is only one energy deposit with three or more crystals.

(2) The ratio of the sum of the energy in the 3×3 crystal matrix (Σ_9) to the sum of energy in the 5×5 crystal matrix (Σ_{25}), corrected for energy losses, must be larger than 0.95.

(3) The polar angle of the deposit lies between 45° and 135°.

(4) The energy of the deposit is greater than 1.5 GeV.

(5) The number of reconstructed TEC tracks is zero.

(6) Less than 1 GeV of energy is deposited in the veto counter.

(7) There is no match between an energy deposit in the veto counter and a deposit in the hadron endcaps.

(8) There is less than 3 GeV in the hadron calorimeter and less than 1 GeV in the low angle part of the endcaps ($<8°$).

(9) The energy deposited in either luminosity monitor is less than 5 GeV.

(10) The event does not satisfy the muon trigger requirements, and no match is found between muon z chamber hits and the BGO deposit.

(11) The skewness of the BGO shower, defined as the ratio between the minor and major axes of the ellipse characterizing the transverse profile of the shower, is larger than 0.2 at 1 GeV, rising linearly to greater than 0.5 at 45 GeV.

Cut (1) eliminates double radiative events, cut (2) ensures that the energy deposit is electromagnetic, cuts (3) and (4) define our acceptance region for the events. Globally the cuts (1)–(11) introduce and inefficiency due to noise of 4%. This inefficiency has been evaluated using beam gate events, single electron events (see below), and radiative dimuon events. There is an additional inefficiency of 5% for photons within the acceptance due to photon conversions, shape cuts, etc. which has been determined from Monte Carlo.

Cuts (5)–(9) reduce the $e^+e^-\gamma$ contamination, cuts (6) and (7) the $\mu\mu\gamma$ events and cut (5) charged pion and single electron backgrounds. Cuts (2), (5) and (11) remove beam–gas or beam–wall events. Cuts (10) and (11) are used to eliminate out of time cosmics on the basis of residual information from the muon chambers and the shower profile in the BGO. Out of time cosmics are a consequence of two constraints coming from the BGO calorimeter: one is the long integration time (8 μs) starting at 2.8 μs before beam crossing, and the other is that the BGO provides no direct information on when the event occurred. This means that an out of time cosmic ray passing through the BGO and emitting a hard photon can simulate a single photon event because the signal it leaves in the rest of the apparatus falls outside the range of full sensitivity. This problem has been solved by using two different methods which are complementary and which achieve nearly 100% efficiency in cosmic background removal when combined. One method, implemented in cut (10), uses the muon z chamber and the muon trigger information, the other, implemented in cut (11), the shape of the BGO energy deposit. The inefficiency from cuts (10) and (11) in the selection of single photon events has been studied using single electron events and found to be 0.7% due to false muon chamber hits coming from noise. The efficiency of these cuts in rejecting cosmics is described below in the section on backgrounds.

After applying these cuts we obtain a sample of 61 events, from which we extract the number of neutrino families.

The total efficiency for the single photon sample includes: the track chamber efficiency of 0.93 due to an inactive TEC sector and independent from the center of mass energy, the cut efficiency against noise of 0.96, the selection efficiency of 0.95, the trigger efficiency which is 0.72 below M_Z+1 GeV and 0.77 above. The total efficiency ranges from 0.60 to 0.67 as a function of the center of mass energy with an error of 0.07.

5. Single electron analysis

Events with a single electron in the BGO barrel, which arise from the reactions $e^+e^-\gamma$ and $e^+e^-\to e^+e^-e^+e^-$, allow us to cross check our single photon selection with a sample one order of magnitude larger and with the same electromagnetic signature. Moreover, we used this larger sample to test the $ee\gamma$ generator, TEEG [13], which also predicts the main background to the $\nu\bar{\nu}\gamma$ signal with a photon in the BGO barrel and the electrons at low forward and backward angles.

To obtain the sample for the single electron analysis, we require cuts similar to the one of the previous section plus a single reconstructed track which is fitted from at least 30 TEC hits and a match in ϕ between the track and the electromagnetic cluster. For comparison with Monte Carlo simulation, additional cuts were applied to isolate the radiative Bhabha events. Firstly, we required a large amount of energy in one of the luminosity detectors ($E_{\mathrm{Lumi}}>30$ GeV) and nothing in the other luminosity detector, the hadron calorimeter endcaps, and veto counter. Secondly, we applied cuts which take advantage of the three-body kinematics of the radiative Bhabha process, namely, once the direction of the unseen particle is assumed, the measurement of the direction and energy of the single electron is sufficient to predict the location of the particle detected in the luminosity detector. Taking the direction of the undetected particle to be 0° (the unseen particle is typically unscattered), it was required that the angular differences between predicted and measured positions of the particle detected in the luminosity detector fall in the following ranges:

$$|\Delta\phi|\leqslant 5^\circ\,,\quad |\Delta\cos\theta|\leqslant 0.0005\,.$$

After these cuts we obtain a sample of 886 events which can be used to check Monte Carlo expectations on $e^+e^-\gamma$. Results are presented in figs. 2 and 2b. The Monte Carlo data has been normalized according to the integrated luminosity and trigger efficiencies with the result that a total of 891 events are expected. The

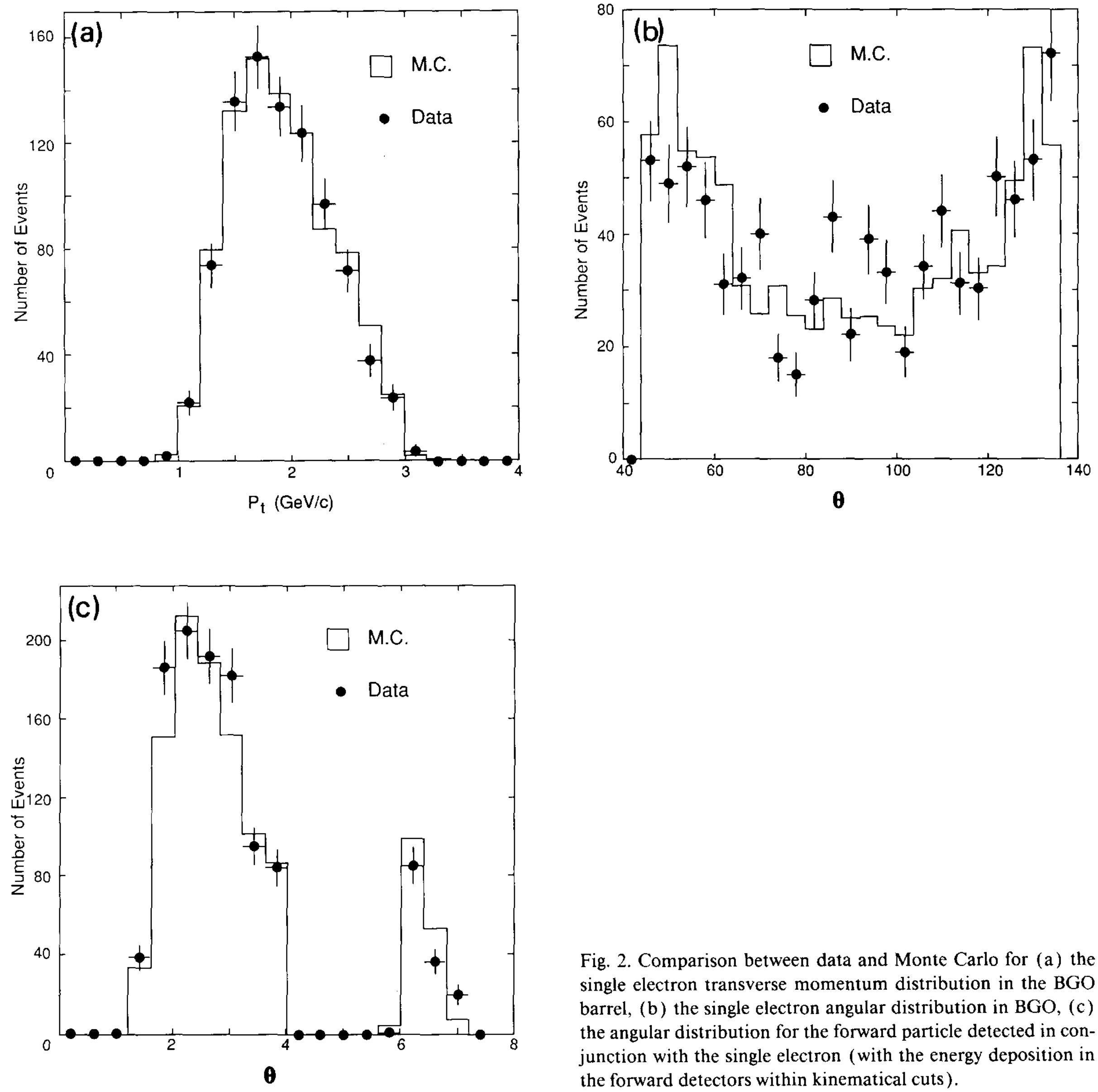

Fig. 2. Comparison between data and Monte Carlo for (a) the single electron transverse momentum distribution in the BGO barrel, (b) the single electron angular distribution in BGO, (c) the angular distribution for the forward particle detected in conjunction with the single electron (with the energy deposition in the forward detectors within kinematical cuts).

agreement gives confidence in the generator to reproduce the $e^+e^-\gamma$ events (with both electrons unseen). Moreover, having weighted the Monte Carlo events with the trigger efficiency curve, this agreement is a positive check on the determination of the trigger efficiency.

Another important point is to verify the correctness of the simulation in the forward region between 3.5° and 10° which includes the gap between the luminosity detector and the endcap hadron calorimeter and the region covered only by the latter (between ~6° and 7°). To do this, we apply the three-body hypothesis cuts on $\Delta\cos\theta$ and $\Delta\phi$ as before but use an energy threshold as low as 1 GeV in the hadron calorimeter endcap. We display in fig. 2c the distribution of the detected electron θ angle for these events compared with the Monte Carlo expectations. The number of events from data is 1126 while the number expected from Monte Carlo, after weighting the events by the trigger efficiencies and normalizing to the integrated luminosity, is 1088 ± 25.

6. Backgrounds to $e^+e^- \to \nu\bar{\nu}\gamma$

6.1. Radiative Bhabha scattering

The dominant background to the $e^+e^- \to \nu\bar{\nu}\gamma$ process comes from the low Q^2 radiative Bhabha scattering when both electrons escape detection and only the photon is seen in our fiducial region. The low angle reach of our luminosity monitors, coupled to the requirement that the photon be inside the BGO barrel with an energy larger than 1.5 GeV, effectively removes $e^+e^-\gamma$ events where both electrons remain in the beam pipe. However, as already pointed out, the scattered electron might not be detected if it escapes into the hole. Because of the kinematical constraints a photon coming from this source will have an energy between 3 and 4.5 GeV, thus giving rise to a false peak at that energy in our data.

To simulate this process we have again used the TEEG Monte Carlo. The simulation allowed both electrons to scatter up to $8°$ in θ, thus giving a total coverage of the luminosity monitor region, the hole, and the low angle part of the endcaps. The behaviour of this Monte Carlo has already been checked using the single electron sample which is the most significant test due to the high statistics of the sample. Two less significant checks were made by comparing the detected number of double-tag luminosity events with a photon in the barrel against the number predicted by Monte Carlo, and the number of single-tag events. The number of double-tag events observed is 9 as compared with 10 expected from Monte Carlo. The number of single-tag events (electron in luminosity monitor or endcap) with a single photon in the BGO barrel are 41 when we expect 29 from Monte Carlo prediction. The agreement is well within the statistical significance of the sample.

Finally, passing the simulated radiative Bhabha events through our single photon selection and weighting the surviving events by the single photon trigger efficiency, we estimate that the sample of 61 candidates contains 7.6 ± 0.8 events of this kind where both electrons are undetected.

6.2. Cosmic rays

To evaluate the level of cosmic contamination in the single photon data sample after our cuts, particularly veto cuts (10) and (11) described above in section 4, we carried out an independent selection of cosmic ray events and then measured the effect of veto cuts (10) and (11) on this sample. The independent selection is based on the BGO analog sums which are used for level-one triggering. Here we take advantage of the fact that the analog signal is sampled in a gate of 2 μs chosen so that if the event is in time the trigger will measure exactly the same energy as the digital readout which is reconstructed offline. Thus the ratio between these two values gives an indication of how much out of time the event was.

Starting then from a sample of 425 single photon candidates obtained before cosmic cuts are applied, we select 180 out of time candidates by requiring that the ratio of the analog sum to the digital sum be less than 0.7. Based on (a) the analysis of our single electrons events, which yields the result that 1.1% of in time electromagnetic showers will have a ratio less than 0.7 and (b) the assumption that the final candidates are dominantly $\nu\bar{\nu}\gamma$ and $e^+e^-\gamma$, we expect 0.7 events in this sample from $\nu\bar{\nu}\gamma$ and $e^+e^-\gamma$. After applying the cosmic cuts (veto cuts (10) and (11)) to this sample of 180 events, one event survives. As 0.7 of it is expected to be an in time signal event and taking into account that the rejection is expected to be even greater for events which are nearly in time, we estimate a contamination of $0.3^{+2.5}_{-0.3}$ event from cosmics.

6.3. Other background processes

Possible backgrounds from other processes have been evaluated by Monte Carlo simulation.

The background from e^+e^- annihilation into three photons, $e^+e^- \to \gamma\gamma\gamma$ [14], contributes 1.0 ± 0.1 event above $E_\gamma > 1.5$ GeV.

The $\mu^+\mu^-\gamma$ final state, where the muons are undetected, contributes less than 0.5 event at the 95% confidence level [15].

Another source of background comes from two-photon processes, $e^+e^- \to e^+e^- X$, where X is a π^0, η, η', a_2, f_2 or a recently-reported high-mass resonance [16] decaying into $\eta\pi^0\pi^0$, when the scattered $e^\pm$ both escape undetected down the beam pipe and only one photon is observed from the final state X. Generation of events was carried out using a Monte Carlo implementation [17] of the cross section formulae found in ref. [18]. Since the two-photon cross section varies little across the Z^0 pole, each sample was generated at $\sqrt{s}=91.2$ GeV. To extend the photon couplings to the resonance from the on-shell photon case to the virtual case, the ρ-pole form factor was used. Resonance decays were generated according to phase space. With the requirement that the photon energy be greater than 1.5 GeV, less than 0.5 event at the 95% confidence is left.

To estimate the background from $e^+e^- \to e^+e^-\ell^+\ell^-\gamma$, we generated samples of events $e^+e^- \to e^+e^-e^+e^-\gamma$ and $e^+e^- \to e^+e^-\mu^+\mu^-\gamma$ at $\sqrt{s}=91.2$ GeV. The event generation is based on the exact lowest-order cross sections [18] for $e^+e^- \to e^+e^-e^+e^-$ and $e^+e^- \to e^+e^-\mu^+\mu^-$ and an algorithm described in ref. [19] to include radiation from the $\ell^+\ell^-$ state. Upper limits of 0.7 events and 0.6 events from $e^+e^- \to e^+e^-e^+e^-\gamma$ and $e^+e^- \to e^+e^-\mu^+\mu^-\gamma$, respectively, are obtained at the 95% confidence level for $E_\gamma > 1.5$ GeV.

In what follows, therefore, we take into account only the background contribution from $e^+e^-\gamma$, $\gamma\gamma\gamma$ and cosmics.

7. Results

Table 1 shows the luminosity, the number of single photon candidates along with the background estimates ($N_{\text{background}} = N^{e^+e^-\gamma}_{\text{expected}} + N^{\gamma\gamma\gamma}_{\text{expected}} + N^{\text{cosmic}}$) at each of the seven center of mass energies. The $N^{\nu\nu\gamma}_{\text{expected}}$ are for $N_\nu=3$, the $N^{\gamma\gamma\gamma}_{\text{expected}}$ and N^{cosmic} are included proportionally to the integrated luminosities.

The measured single photon energy distributions are shown in fig. 3 along with Monte Carlo predictions for the process $e^+e^- \to \nu\bar{\nu}\gamma$, with three families of light neutrinos, and for the background from the $e^+e^- \to e^+e^-\gamma$ source. For $\nu\bar{\nu}\gamma$ we have used the NNGSTR program using the full second order corrections [20]. These plots show good agreement between data and Monte Carlo as well as fig. 4 where we show the θ distribution for our candidates.

The corrected cross sections for the process $e^+e^- \to \nu\bar{\nu}\gamma$ are shown in the last column of table 1 for the case that one photon is above 1.5 GeV in the angular region $|\cos\theta| < 0.7$ with no restrictions on additional photons. These are calculated from the observed number of events, the integrated luminosity and the background contributions shown in table 1, applying the efficiency given in section 4. The errors represent 68% CL intervals and take into account the background fluctuations [21].

We extract the number of families of light neutrinos N_ν from our sample, by performing a maximum likelihood fit to the number of candidates, for the seven center of mass energy points as shown in table 1. We use Poisson probabilities, calculated as a func-

Table 1
Luminosity, observed and expected number of events corrected cross sections for $e^+e^- \to \nu\bar{\nu}\gamma$ at each center of mass energy.

E_{cm} (GeV)	L (nb^{-1})	N_{observed}	$N^{\nu\nu\gamma}_{\text{expected}}$	$N_{\text{background}}$	σ (pb)
88.28	215	–	0.5	0.7	$0+14$
89.28	226	3	0.8	0.7	17^{+21}_{-12}
90.28	132	2	0.7	0.3	21^{+34}_{-17}
91.28	1481	15	16.2	4.5	11^{+5}_{-4}
92.28	245	4	5.2	0.7	22^{+21}_{-12}
93.28	334	15	11.3	0.9	70^{+25}_{-19}
94.28	347	22	14.7	1.0	90^{+25}_{-20}
total	2980	61	49.4	8.8	

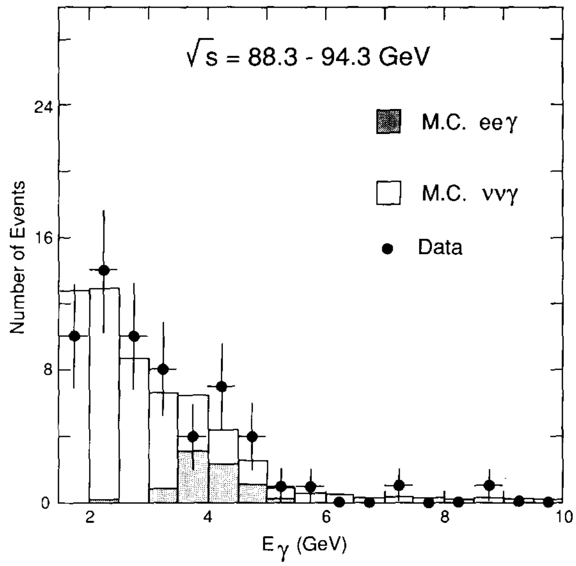

(a)

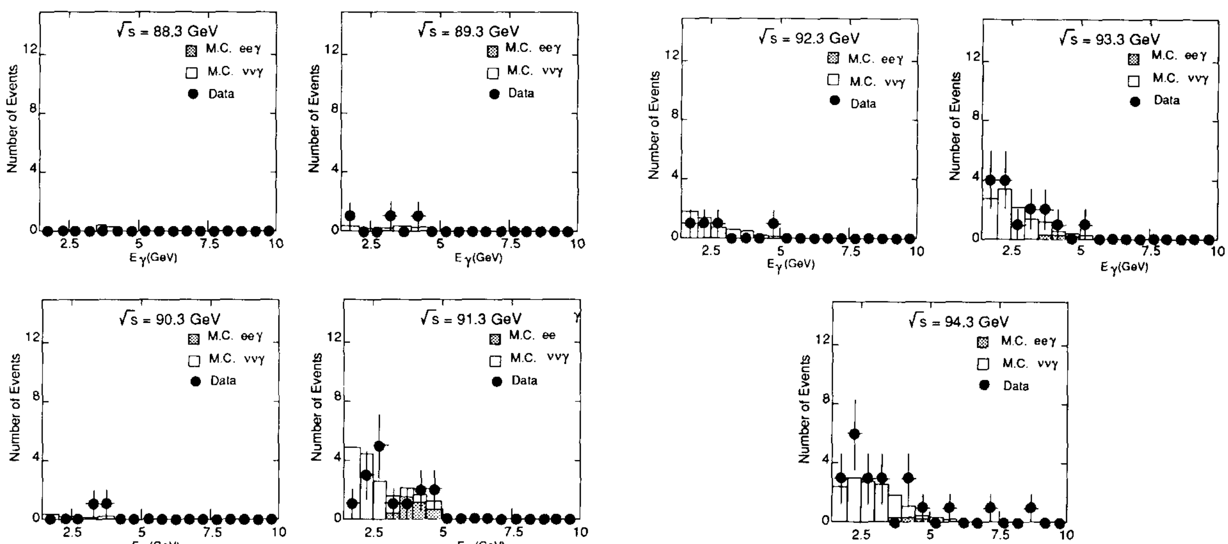

(b)

tion of the expected number of signal and background events. For the $e^+e^- \to \nu\bar{\nu}\gamma$ process, taking into account the trigger efficiency and the selection requirements, we computed, for each CM energy, the effective cross section corresponding to N_ν between 2 and 4 and used a straight line fit to get a parametrization of the cross section dependence on N_ν. The effective cross section was calculated using and analytical program [22]. We have modified this program using an improved Born approximation of eq. (2) with an s-dependent Z^0 width to account for the electro-weak radiative corrections. The cross section (2) is written as

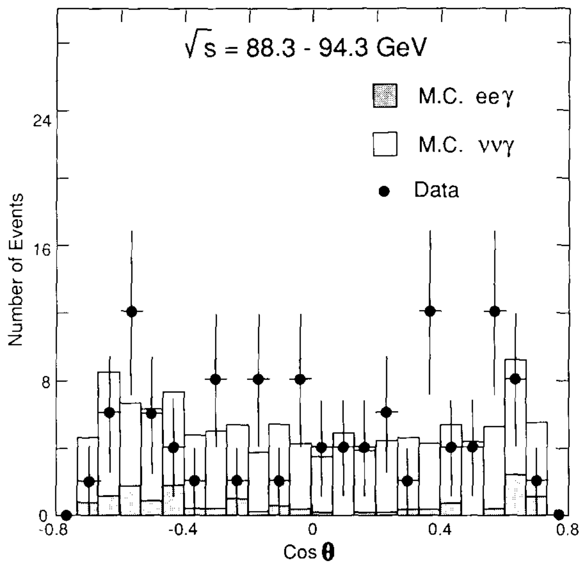

Fig. 4. cos θ distributions for single photon candidates.

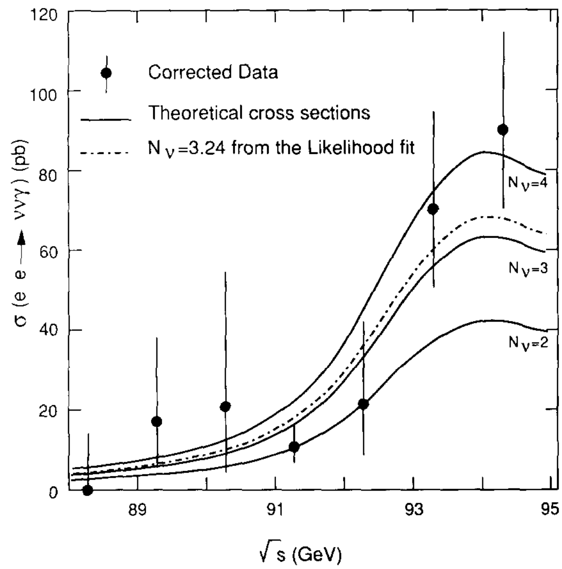

Fig. 5. Corrected cross section (pb) as a function of CM energy. The solid curves show the expectations from $N_\nu=2$, 3, 4 and the dashed one what is obtained with our best fit ($N_\nu=3.24\pm0.46$).

$$\sigma_0(s)=\frac{12\pi}{M_Z^2}\,\frac{s\Gamma_e N_\nu \Gamma_\nu}{(s-M_Z^2)^2+s^2\Gamma_Z^2/M_Z^2}+\mathrm{W\ terms}\,, \tag{3}$$

where Γ_ν is the standard model Z^0 partial width for each neutrino family and M_Z, Γ_Z, and Γ_e are respectively the Z^0 mass, total width, and electron partial width.

The agreement, for $N_\nu=3$, of this program with NNGSTR is better than 1%. To describe the Z^0 resonance we used as input parameters our most recent measurements [23], $M_Z=91.181\pm0.010\pm0.02$ [LEP] GeV and $\Gamma_Z=2.501\pm0.017$ GeV. Moreover, Γ_e is defined from our measured value $\sin^2\bar{\theta}_w=0.227^{+0.008}_{-0.006}$. In this approach we then allow the parameter N_ν to vary while keeping the total width fixed.

The result we find is $N_\nu=3.24\pm0.46$ (stat.).

It is worth noting here that if we take

$$\Gamma_Z=\Gamma_h^{SM}+3\Gamma_e^{SM}+\Gamma_{inv.}\,, \tag{4}$$

where $\Gamma_{inv.}=N_\nu\Gamma_\nu^{SM}$ is the invisible width and Γ_h^{SM}, Γ_e^{SM}, Γ_ν^{SM} are calculated from the standard model and we allow Γ_Z to vary with N_ν in the fit, we get $N_\nu=3.24\pm0.62$ (stat.).

Contributions to the systematic error in our analysis come from the luminosity which gives an uncertainty on the number of families of $\Delta N_\nu=\pm0.03$, the selection efficiency, $\Delta N_\nu=\pm0.06$, the determination of the trigger efficiency, $\Delta N_\nu=\pm0.16$, and the cosmic contamination, $\Delta N_\nu={}^{+0.13}_{-0.02}$. Moreover, the errors from M_Z, Γ_Z and $\sin\bar{\theta}_w$, from the top mass variation and from the theoretical uncertainty, give a total contribution of $\Delta N_\nu=\pm0.07$. Adding all these systematic errors in quadrature, we estimate the total systematic error to be $\Delta N_\nu=\pm0.22$ family. Our final result then is

$$N_\nu=3.24\pm0.46(\mathrm{stat.})\pm0.22(\mathrm{syst.})\,.$$

This corresponds to an invisible width of the Z^0 of $540\pm80\pm40$ MeV once we assume that the only invisible decay modes are to light neutrinos and we use the standard model value of $\Gamma_\nu^{SM}=166.8\pm1.5$ MeV for the partial decay width into a single light neutrino family. (The uncertainty in the standard model partial width is obtained by varying the top mass between 90 and 250 GeV and the Higgs mass between 45 and 1000 GeV.) This is in agreement with the result published by the OPAL Collaboration in a similar analysis [24]. The corrected cross section is shown as a function of CM energy in fig. 5 along with the expectations from $N_\nu=2$, 3, 4 and for the likelihood fit.

8. Conclusion

A direct determination of the number of light neutrino families is performed by measuring the single photon cross section at center of mass energies near the Z^0 resonance with the L3 detector assuming the standard model Z^0 coupling to neutrinos. A total of 61 events with photon energies larger than 1.5 GeV are observed for a corresponding integrated luminosity of 3.0 pb^{-1}. A maximum likelihood fit gives $N_\nu = 3.24 \pm 0.46 \pm 0.22$. This is in agreement with the L3 result of $N_\nu = 3.05 \pm 0.10$ from the line shape method [22].

Acknowledgement

We wish to express our gratitude to the CERN accelerator divisions for the excellent performance of the LEP machine. We acknowledge the effort of all engineers and technicians who have participated in the construction and maintenance of this experiment.

References

[1] ALEPH Collab., D. Decamp et al., CERN preprint CERN-PPE/91-105 (1991);
DELPHI Collab., P. Abreu et al., CERN preprint CERN-PPE/91-95 (1991);
L3 Collab., B. Adeva et al., Z. Phys. C 51 (1991) 179;
OPAL Collab., G. Alexander et al., CERN preprint CERN-PPE/91-67 (1991).

[2] A.D. Dolgov, L.B. Okun and V.I. Zakharov, Nucl. Phys. B 41 (1972) 197;
E. Ma and J. Okada, Phys. Rev. Lett. 41 (1978) 287;
K.J. Gaemers, R. Gastmans and F.M. Renard, Phys. Rev. D 19 (1979) 1605;
G. Barbiellini, B. Richter and J. Siegrist, Phys. Lett. B 106 (1981) 414.

[3] L. Trentadue et al., in: Z. Physics at LEP 1, ed. G. Altarelli, CERN yellow report CERN 89-08 (CERN, Geneva, 1989), p. 129.

[4] MAC Collab., W.T. Ford et al., Phys. Rev. D 33 (1986) 3472;
ASP Collab., C. Hearty et al., Phys. Rev. D 39 (1989) 3207.

[5] H. Wu, Ph.D. thesis, Universität Hamburg (1986), unpublished;
CELLO Collab., H.-J. Behrend et al., Phys. Lett. B 215 (1988) 186.

[6] VENUS Collab., K. Abe et al., Phys. Lett. B 232 (1989) 431.

[7] M. Chen et al., Phys. Rep. 159 (1988) 201.

[8] L3 Collab., B. Adeva et al., Nucl. Instrum. Methods A 289 (1990) 35.

[9] R. Brun et al., GEANT3 Users Guide, CERN report CERN/DD/EE/84.1.

[10] H. Fesefeldt, RWTH Aachen Report PITHA 85/02 (1985).

[11] LeCroy Corporation, Nuclear Products Catalog (1990).

[12] R. Bizarri et al., Nucl. Instrum. Methods A 283 (1989) 799.

[13] D. Karlen, Nucl. Phys. B 289 (1987) 23.

[14] F.A. Berends and R. Kleiss, Nucl. Phys. B 186 (1981) 22.

[15] S. Jadach, B.F.L. Ward and Z. Was, KORALZ, CERN preprint TH 5994-91 (1991).

[16] K. Karch et al., Phys. Lett. B 249 (1990) 353.

[17] F.L. Linde, Ph.D. Thesis, Rijksuniversiteit Leiden (1988).

[18] V.M. Budnev et al., Phys. Rep. 15 (1975) 181.

[19] R. Kleis, Phys. Lett. B 180 (1986) 400.

[20] R. Miquel, C. Mana and M. Martinez, Z. Phys. C48 (1990) 309;
F.A. Berends et al., Nucl. Phys. B 301 (1988) 583.

[21] Particle Data Group, J.J. Hernández et al., Review of particle properties, Phys. Lett. B 239 (1990) 1.

[22] O. Nicrosini and L. Trentadue, Nucl. Phys. B 318 (1989) 1.

[23] L3 Collab., B. Adeva et al., Z. Phys. C 51 (1991) 179.

[24] OPAL Collab., M.Z. Akraway et al., Z. Phys. C 50 (1991) 373.